1521-0111/12/8102-175–188$25.00
MOLECULAR PHARMACOLOGY
Vol. 81, No. 2
74088/3742130

Mol Pharmacol 81:175–188, 2012

$\alpha7\beta2$ Nicotinic Acetylcholine Receptors Assemble, Function, and Are Activated Primarily via Their $\alpha7$-$\alpha7$ Interfaces[S]

Teresa A. Murray, Daniel Bertrand, Roger L. Papke, Andrew A. George, Rigo Pantoja, Rahul Srinivasan, Qiang Liu, Jie Wu, Paul Whiteaker, Henry A. Lester, and Ronald J. Lukas

Barrow Neurological Institute, Phoenix, Arizona (T.A.M., A.A.G., Q.L., J.W., P.W., R.J.L.); Biomedical Engineering Department, Louisiana Tech University, Ruston, Louisiana (T.A.M.); Division of Biology, California Institute of Technology, Pasadena, California (R.P., R.S., H.A.L.); Department of Neuroscience, Centre Médical Universitaire, and HiQScreen Sàrl, Geneva, Switzerland (D.B.); and Department of Pharmacology and Therapeutics, College of Medicine, University of Florida, Gainesville, Florida (R.L.P.)

Received June 12, 2011; accepted October 28, 2011

ABSTRACT

We investigated assembly and function of nicotinic acetylcholine receptors (nAChRs) composed of $\alpha7$ and $\beta2$ subunits. We measured optical and electrophysiological properties of wild-type and mutant subunits expressed in cell lines and *Xenopus laevis* oocytes. Laser scanning confocal microscopy indicated that fluorescently tagged $\alpha7$ and $\beta2$ subunits colocalize. Förster resonance energy transfer between fluorescently tagged subunits strongly suggested that $\alpha7$ and $\beta2$ subunits coassemble. Total internal reflection fluorescence microscopy revealed that assemblies localized to filopodia-like processes of SH-EP1 cells. Gain-of-function $\alpha7$ and $\beta2$ subunits confirmed that these subunits coassemble within functional receptors. Moreover, $\alpha7\beta2$ nAChRs composed of wild-type subunits or fluorescently tagged subunits had pharmacological properties similar to those of $\alpha7$ nAChRs, although amplitudes of $\alpha7\beta2$ nAChR-mediated, agonist-evoked currents were generally ~2-fold lower than those for $\alpha7$ nAChRs. It is noteworthy that $\alpha7\beta2$ nAChRs displayed sensitivity to low concentrations of the antagonist dihydro-β-erythroidine that was not observed for $\alpha7$ nAChRs at comparable concentrations. In addition, cysteine mutants revealed that the $\alpha7$-$\beta2$ subunit interface does not bind ligand in a functionally productive manner, partly explaining lower $\alpha7\beta2$ nAChR current amplitudes and challenges in identifying the function of native $\alpha7\beta2$ nAChRs. On the basis of our findings, we have constructed a model predicting receptor function that is based on stoichiometry and position of $\beta2$ subunits within the $\alpha7\beta2$ nAChRs.

Introduction

Nicotinic acetylcholine receptors (nAChRs) are members of the ligand-gated ion channel superfamily of neurotransmitter receptors. They exist as a collection of subtypes, each composed as a pentamer of homologous protein subunits. Each nAChR subtype has characteristic ion selectivity, channel gating kinetics, ligand recognition features, and cellular/subcellular distribution. Several predominant mammalian nAChR subtypes ($\alpha1\beta1\gamma\delta/\varepsilon$, $\alpha4\beta2$*, $\alpha7$ homopentamers) have been studied extensively, revealing involvement in functions such as neuromuscular signaling, mood, memory, attention,

This work was supported by the National Institutes of Health National Institute on Drug Abuse [Grants DA015389, DA027070, DA012242]; the National Institutes of Health National Institute of Neurological Diseases and Stroke [Grant NS11756]; the National Institutes of Health National Institute of Mental Health [Grant MH086383]; the National Institutes of Health National Institute of General Medical Sciences [Grant GM057481]; a US National Science Foundation Graduate Research Fellowship; the Barrow Neurological Foundation; a Catholic Healthcare West SEED Grant; the Biodesign Institute at Arizona State University, the Swiss National Science Foundation; the EC Neurocypres Grant; and the California Tobacco-Related Disease Research Program.

Article, publication date, and citation information can be found at http://molpharm.aspetjournals.org.

http://dx.doi.org/10.1124/mol.111.074088.

[S] The online version of this article (available at http://molpharm.aspetjournals.org) contains supplemental material.

ABBREVIATIONS: nAChR, nicotinic acetylcholine receptor; MS/DB, medial septum-diagonal band; YFP, yellow fluorescent protein; CFP, cyan fluorescent protein; GluCl, glutamate-gated chloride channel; $\alpha4$Y, YFP-tagged nAChR $\alpha4$ subunit; $\alpha7$C YFP-tagged nAChR $\alpha7$ subunit; $\alpha7$Y, CFP-tagged nAChR $\alpha7$ subunit; $\beta2$C, CFP-tagged nAChR $\beta2$ subunit; $\beta2$Ch, mCherry-tagged nAChR $\beta2$ subunit; GCαY, YFP-tagged glutamate-gated chloride channel α subunit; GCβC, CFP-tagged glutamate-gated chloride channel β subunit; LSCM, laser scanning confocal microscopy; FRET, Förster resonance energy transfer; TIRF, total internal reflection fluorescence; BAPTA, 1,2-bis(2-aminophenoxy)ethane-*N*,*N*,*N*′,*N*′-tetraacetic acid; MTSEA, methanethiosulfonate ethylammonium; ACh, acetylcholine; MLA, methyllycaconitine; FP, fusion protein; ER, endoplasmic reticulum; ROI, region of interest; DHβE, dihydro-β-erythroidine; PNU-282987, *N*-(3*R*)-1-azabicyclo[2.2.2]oct-3-yl-4-chlorobenzamide; *E*, FRET efficiency; I_D, intensity of donor FP after photodestruction of acceptor; I_{DA}, intensity of donor FP in the presence of the unbleached acceptor; I_n, normalized fluorescence intensity.

addiction, and pathologic conditions (as reviewed in Le Novère et al., 2002). Deneris et al. (1988) reported the discovery of the β2 subunit and suggested that diverse nAChRs could result from coassembly with different α subunits. Indeed, reports since have shown that β2 coassembles with α2-α4 and/or α6, each yielding distinct functional characteristics (Marks et al., 1999; Drenan et al., 2008). Ligand binding domains are thought to reside at specific interfaces between positive faces of α subunits and apposed, negative faces of neighboring subunits; work continues to identify which interfaces are functional (Lukas and Bencherif, 2006). However, subunits that do not directly participate in ligand binding domains can still influence function, such as ligand sensitivity (Luetje and Patrick, 1991), desensitization (Bohler et al., 2001), sensitivity to inhibitors, and permeability (Francis and Papke, 1996).

Most receptors are heteromeric; however, evidence suggests that α7 subunits predominantly form homopentameric α7 nAChRs when naturally or heterologously expressed (Couturier et al., 1990). Additional evidence suggests that other nAChR subunits can combine with α7 to form heteromeric, α7* nAChRs (where * indicates other nAChR subunit assembly partners) when transiently expressed in *Xenopus laevis* oocytes (Palma et al., 1999; Khiroug et al., 2002) or naturally expressed in nonmammalian systems such as embryonic chick neurons (Gotti et al., 1994) and chick brain (Anand et al., 1993). Furthermore, some evidence supports heteromeric mammalian α7* nAChRs expression. For example, Zarei et al. (1999) found that although α7 and β2 subunits in cultured hippocampal neurons had distinctive patterns of localization, partial overlapping distribution on cell soma suggested heteromeric receptors could exist. Later, Khiroug et al. (2002) coimmunoprecipitated α7 and β2 subunits from cotransfected TSA201 cells, demonstrating the potential for coassembly in mammalian cells. Subsequently, Azam et al. (2003) found that several subpopulations of neurons in rat brain coexpress α7 and β2 subunit mRNAs but not α4 mRNA, the most common β2 subunit assembly partner, further supporting the possibility of mammalian α7β2 nAChRs. Most recently, Liu et al. (2009) identified a unique class of functional nAChRs in cholinergic neurons of the rodent medial septum-diagonal band (MS/DB) that appear to contain both α7 and β2 subunits using wild-type and β2 subunit knockout mice. Moreover, they discovered that these receptors were inhibited by pathologically relevant levels of amyloid β_{1-42} (Aβ) peptide, suggesting that they may be important in the pathogenesis of Alzheimer's disease.

The current study exploited fluorescently tagged nAChR α7 and β2 subunits to characterize α7β2 nAChR formation, functional mutants to investigate α7 and β2 subunits coassembly, wild-type subunits to probe pharmacological differences between α7 and α7β2, and cysteine mutants to identify functional binding sites.

Materials and Methods

cDNA Construction and cRNA Preparation

Mouse cDNA Constructs. cDNA constructs have been described previously for mouse nAChR α7 subunits and yellow fluorescent protein (YFP)-tagged α7 subunits (α7Y; Murray et al., 2009); for cyan fluorescent protein (CFP)- or YFP-tagged mouse nAChR β2 subunits (β2C and β2Y, respectively) and YFP-tagged mouse nAChR α4 subunits (α4Y; Nashmi et al., 2003); and for YFP-tagged glutamate-gated chloride channel (GluCl) α subunits (GCαY) and CFP-tagged β subunits (GCβC; Slimko and Lester, 2003). The nAChR β2 subunit-mCherry fusion protein (β2Ch) was made as described previously (Nashmi et al., 2003) except with mCherry inserted as the FP. For all nAChR subunit-FP constructs, the FP sequence was inserted into the sequence coding for the nAChR subunit's large, intracellular/cytoplasmic, C2 loop between M3 and M4. This loop is not thought to be involved in channel gating and/or ligand recognition; and the insertion site was chosen to avoid disrupting predicted consensus sequences for phosphorylation, trafficking or other potentially important sites (Nashmi et al., 2003; Murray et al., 2009). The β2C construct was excised from the vector pCI-neo with EcoRI and inserted into the vector pcDNA3.1-zeo. RIC-3 cDNA was generously provided by Dr. Millet Treinin (Hebrew University, Jerusalem, Israel) through Dr. William Green (University of Chicago, Chicago, IL).

Construction and Subcloning of a CFP-Tagged nAChR α7 Subunit cDNA. Primers were designed to amplify the *CFP* gene, including an upstream c-Myc tag, using the β2C construct (Nashmi et al., 2003) as a template. The forward and reverse primer sequences were 5′-CGT GTG TGG TCG TTT GGC CTG CGA GCA GAA GCT GAT CTC AG-3′ and 5′-GGT GCT CAT CAT GTG TTG GGG ACT TGT ACA GCT CGT CCA TGC-3′, respectively. These primers added overhangs complementary to the mouse nAChR α7 subunit cDNA on either side of the fluorescent tag insertion site at the same sequence position at which YFP was inserted into α7Y (Murray et al., 2009). A second polymerase chain reaction was performed with this CFP construct and the mouse α7 subunit cDNA in pcDNA3.1^{+}-hygro (the latter serving as the destination vector in a 5:1 mass ratio of construct to vector).

Mouse cDNA and cRNA Preparation for Oocyte Injection. The cDNAs of mouse wild-type α7 (mα7) and α7-yellow fluorescent protein (mα7-YFP; originally denoted α7 and α7Y, respectively; Murray et al., 2009) were subcloned into the vector pGEMHE. wild-type β2 (mβ2) cDNA was provided by Jerry Stitzel (University of Colorado, Boulder, CO), and the β2 gain-of-function mutant ($\beta2^{V9'S}$) was provided by Bhagirathi Dash (Barrow Neurological Institute, Phoenix, AZ) and generated using a QuikChange kit (Stratagene, La Jolla, CA). β2 subunit constructs were also subcloned into the pGEMHE vector. After linearizing plasmids with NheI (2 h at 37°C) and treatment with proteinase K (30 min at 50°C), cRNAs were transcribed using mMessage mMachine T7 kit (Applied Biosystems/Ambion, Austin, TX). Reactions were treated with TURBO DNase (1 U for 15 min at 37°C), and cRNAs were purified using the RNeasy Clean-up kit (QIAGEN, Valencia, CA). cRNAs were confirmed on a 1% agarose gel and stored at −80°C.

Human nAChR Cysteine Mutants and Clones. The wild-type human nAChR clones were provided by Dr. Jon Lindstrom (University of Pennsylvania, Philadelphia, PA). Mutations to cDNA clones were introduced using the QuikChange kit (Stratagene) according to the manufacturer's instructions. The mutations were confirmed with automated fluorescent sequencing. After linearization and purification of cloned cDNAs, RNA transcripts were prepared in vitro using the appropriate mMessage mMachine kit (Ambion, Inc.).

Subunit Expression

Cell Culture, Creation of Stably Transfected SH-EP1 Cell Lines, and Transient Transfections. SH-EP1 human epithelial cells were stably transfected to heterologously express FP-tagged nAChR subunit(s) or were used for transient transfections, as described previously (Murray et al., 2009). Previous studies have shown that SH-EP1 cells are native nAChR-null, making them potentially good hosts for heterologous expression of nAChRs, as has been demonstrated (Wu et al., 2006; Murray et al., 2009). For stably transfected cell lines, final concentrations of antibiotics were hygromycin B (170 μg/ml; Calbiochem, San Diego, CA) for α7Y and α7C, G418 (480 μg/ml; A.G. Scientific, San Diego, CA) for α4Y, or phleomycin (Zeocin; 260 μg/ml; Invitrogen Corp., Carlsbad, CA) for β2C.

SH-EP1 cells expressing α7Y or α7C alone, α7Y with β2C, or α4Y with β2C were from stably transfected cell lines. Transient transfection was used to generate cells expressing other nAChR subunits, GluCl subunits, and/or RIC-3. In preliminary experiments for transfection of RIC-3, we found that comparatively low amounts of cDNA (100–300 ng) gave maximal surface expression of nicotinic receptors. Higher and lower amounts of cDNA seemed to decrease surface expression and were not used; Alexander et al. (2010) independently found similar results. Cells requiring transient transfections for microscopy were seeded 24 h before transfection. Fluorescence developed ~12 h after transfection and began declining after 48 h; therefore, transiently transfected cells were studied within 16 to 48 h after transfection.

Oocyte Preparation and Mouse RNA Injection. Female *X. laevis* (Xenopus I, Ann Arbor, MI) were anesthetized by 0.2% 3-aminobenzoic acid ethyl ester (MS-222; Sigma-Aldrich, St. Louis MO). The ovarian lobes were surgically removed from the frog and placed in calcium-free OR2 incubation solution consisting of 92.5 mM NaCl, 2.5 mM KCl, 1 mM $MgCl_2$, 1 mM Na_2HPO_4, 5 mM HEPES, 50 U/ml penicillin, and 50 μg/ml streptomycin, pH 7.5. The lobes were cut into small pieces and digested with 0.75 U/ml Liberase Thermolysin medium (Roche Pharmaceuticals, Nutley, NJ) with constant stirring at room temperature for 1 h. The dispersed oocytes were thoroughly rinsed with the above solution containing 1 mM $CaCl_2$. Stage VI oocytes were selected and incubated at 13°C.

Micropipettes for RNA injection were pulled from filamented borosilicate glass (Drummond Scientific, Broomall, PA) on a horizontal puller (P87; Sutter Instruments, Novato, CA), and the tips were broken with an outer diameter ≅ 40 μm (resistance, 2–6 mΩ). A Nanoject microinjection system (Drummond Scientific) was used to inject 20 to 60 nl containing ~1 ng of RNA.

Human nAChR Wild-Type and L9′T Reporter Subunit Expression. To assess properties of human α7 subunits alone or in combination with wild-type or mutated human nAChR β2 subunits, a total of 2 ng of cDNAs encoding α7 and β2 subunits was injected (10 nl) into the nucleus of *X. laevis* oocytes using an automated injection device (RoboInject, Multichannel Systems, MCS GmbH, Reutlingen, Germany; Hogg et al., 2008). Human nAChR α7 and β2 subunit cDNA constructs were kindly provided, respectively, by Dr. Christian Fuhrer (University of Zurich, Zurich, Switzerland) and Prof. Dr. Ortrud K. Steinlein (Ludwig-Maximilians-University of Munich, Munich, Germany). L9′T mutant α7 and β2 subunits were generated by standard, single nucleotide substitution using commercially available kits. After injection, cells were maintained for 2 or more days in a sterile Barth solution containing 88 mM NaCl, 1 mM KCl, 2.4 mM $NaHCO_3$, 10 mM HEPES, 0.82 mM $MgSO_4 \cdot 7H_2O$, 0.33 mM $Ca(NO_3)_2 \cdot 4H_2O$, and 0.41 mM $CaCl_2 \cdot 6H_2O$, at pH 7.4, and supplemented with 100 unit/ml penicillin and 100 μg/ml streptomycin.

Expression of Cysteine Mutants in *X. laevis* Oocytes. Methods of oocyte harvesting, preparation, and injection have been described previously (Williams et al., 2011). In brief, stage 5 oocytes were injected with 50 nl (5–20 ng) each of the appropriate RNAs. Recordings were made 2 to 7 days after injection.

Microscopy

Laser Scanning Confocal Microscopy. A Nikon C1 LSCM (Nikon Instruments Inc., Melville, NY), with a spectral imaging system was used to acquire fluorescence spectra (λ stacks, 5 nm per detector, 32 detectors) in live cells containing fluorescently tagged proteins, as described previously (Drenan et al., 2008) using a 6.72-μs pixel dwell time and a 60-μm pinhole diameter. Linear unmixing was used offline, as previously described, to separate the overlapping fluorescence spectra. Unmixed images were pseudocolored, the dark level was adjusted to reduce background noise, and saturation was adjusted for YFP and CFP in the same amount for each image set and then merged to determine colocalization (Nikon EZ-C1 Viewer; the γ control was not adjusted).

Förster Resonance Energy Transfer Microscopy. FRET detection was accomplished by the acceptor photobleaching method, as described previously (Nashmi et al., 2003; Drenan et al., 2008). In brief, when a YFP-tagged protein is interacting with a CFP-tagged protein, such as is the case with subunit coassembly, incremental photodestruction (photobleaching) of YFP by strong laser light results in a stepwise decrease in the intensity of YFP fluorescence with a concurrent increase in the intensity of CFP fluorescence. Linear unmixing was used to separate the overlapping emission spectra of CFP and YFP before calculating FRET efficiency. FRET efficiency (E) was calculated as follows: $E = [1 - (I_{DA}/I_D)] \times 100\%$, where I_{DA} represents the donor intensity in the presence of the acceptor before bleaching the acceptor, and I_D is the theoretical intensity of the donor without the acceptor. Prebleach intensities were normalized to 100%. To minimize effects of collateral donor bleaching, the acceptor was not completely bleached. Instead, I_D was extrapolated from a linear fit to a scatter plot of the fractional change in normalized donor intensity versus the normalized acceptor intensity (e.g., Fig. 2, B).

Total Internal Reflection Fluorescence Microscopy. Cellular autofluorescence was minimized by removing cell culture medium and replacing it with extracellular imaging solution and imaged using an Olympus TIRF system, as described previously (Drenan et al., 2008). For determination of colocalization, the single Optosplit image, which recorded the mCherry and YFP channel images side by side, was partitioned into two separate images using the Cairn Image Splitter plug-in for Image J (http://rsbweb.nih.gov/ij/). These were then merged to reveal colocalized subunits in the same manner as LSCM images, described above.

Electrophysiology

Human nAChR Wild-Type and L9′T Mutant Subunits Expressed in Oocytes. All recordings were performed at 18°C and cells were superfused with OR2 medium containing 82.5 mM NaCl, 2.5 mM KCl, 5 mM HEPES, 1.8 mM $CaCl_2 \cdot 2H_2O$, and 1 mM $MgCl_2 \cdot 6H_2O$, pH 7.4. Cells were impaled using a two-electrode voltage-clamp system with a HiClamp (Multi Channel Systems, Reutlingen, Germany) automated recording system. Electrodes were filled with 3 M KCl. Cells were held at −100 mV throughout the experiments. Data were digitized at least at 100 Hz, captured on a PC, and analyzed using MATLAB (The Mathworks, Inc., Natick, MA). Cells were treated for at least 3 h with the calcium chelating agent BAPTA-acetoxymethyl ester to suppress the possible contamination by calcium activated chloride currents. Measurements for each agonist were carried out in sibling oocytes to improve the consistency of receptor expression.

To explore the possible assembly of β2 subunits within the α7 receptor complex, the gain-of-function mutation L9′T, initially reported as L247T in the chick α7 (Revah et al., 1991) was used as a reporter mutation. In some experiments, the 1:1 ratio of cDNA encoding for α7 and β2 subunits was modified (as indicated on Fig. 5) to increase the level of expression of β2 subunits; consequently, its probability of insertion into functional receptors. All compounds were freshly prepared on the day of each experiment.

Cysteine Mutants. Experiments were conducted using OpusXpress 6000A (Molecular Devices, Union City, CA) as described by Stokes et al. (2004). Flow rates were set at 2 ml/min for experiments with α7 receptors and 4 ml/min for other subtypes. Methanethiosulfonate ethylammonium (MTSEA) was purchased from Toronto Research Chemicals Inc. (North York, ON, Canada). All other chemicals for electrophysiology were obtained from Sigma-Aldrich (St. Louis, MO). Fresh ACh and sulfhydryl reagent stock solutions were made daily in Ringer's solution and diluted.

Each oocyte received two control applications of ACh (300 μM), followed by incubation with MTSEA, and then application of ACh. The peak amplitude and the net charge (Papke and Porter-Papke, 2002) of responses were normalized to the preceding ACh control responses, compensating for the varied levels of channel expression between oocytes. Although the absolute magnitude of the evoked current responses increased over time, the normalized values of the responses did not vary significantly over time.

The time interval between repeated applications of 300 μM ACh was 3 min. Although desensitization of α7-mediated responses is rapid during an agonist application, it is also very rapidly reversed once agonist is washed from the chamber (Williams et al., 2011). There was no progressive desensitization, and the magnitude of ACh-evoked controls was consistent throughout the experiments unless sulfhydryl reagents were applied to receptors containing L119C mutant α7 receptor subunits.

Fluorescently Tagged Mouse nAChR Subunits Expressed in SH-EP1 Cells. Patch-clamp whole-cell current recording, coupled with computer-controlled two-barrel application and removal of agonists was used, as described previously (Wu et al., 2006). In brief, the decline in choline-induced current over the course of agonist application was analyzed for decay time constant ($\tau = 0.693/k$ for decay rate constant k), peak current (I_p), and steady-state current (I_s), using fits to the single (or double) exponential expression $I = ([I_p - I_s]\, e^{-k\tau}) + I_s$ or $I = ([I_p - I_i]\, e^{-k_1\tau}) + ([I_i - I_s]\, e^{-k_2\tau}) + I_s$, where I_i is the intermediate level of current and k_1 and k_2 are rate constants for the two decay processes. Concentration-response profiles were fit to the Hill equation using Prism 3.0 (GraphPad Software, Inc., San Diego, CA). Choline and methyllycaconitine (MLA) were supplied by Sigma-Aldrich.

Mouse nAChR Subunits Expressed in Oocytes. Ten days after injection, oocytes expressing nAChR subunits were voltage-clamped at −70 mV with an Axoclamp 900A amplifier (Molecular Devices, Sunnyvale, CA). Recordings were sampled at 10 kHz (low-pass Bessel filter, 40 Hz; high-pass filter, direct current), and the resulting traces were saved to disk (Clampex ver. 10.2; Molecular Devices). Oocytes with leak currents (I_{leak}) > 60 nA were immediately excluded from recordings. Dose-response relationships were determined by measuring the current induced by a range of acetylcholine concentrations (10 μM–10 mM; half-log units). Data were analyzed using one-way analysis of variance and Tukey's multiple comparison test for testing for comparing the means of three or more treatment groups or nonlinear comparisons for dose-response relationships (Prism).

Data Analysis. Unless otherwise noted, pairwise t tests were used to compare mean values using the assumption of normality and equal variance. Significance was established at $p < 0.05$. Summary data are reported as the mean ± S.E.M.

Results

Fluorescently Labeled Subunits Used to Probe α7 and β2 Coassembly

Confocal Microscopy Shows Colocalization of FP-Tagged α7Y and β2C Subunits. LSCM was employed to determine whether nAChR α7 and β2 subunits colocalize in mammalian cells. To facilitate this study, α7 subunits with a YFP fusion (α7Y) and β2 subunits with a CFP fusion (β2C) were heterologously and stably expressed in the native nAChR-null SH-EP1 human cell line (α7Yβ2C cells). Control SH-EP1 cell lines also were created that stably expressed α7Y alone (α7Y cells; Murray et al., 2009) or nAChR α4-YFP and β2-CFP fusion subunits (α4Yβ2C cells). LSCM images were acquired over the spectral range of CFP and YFP emission (λ stacks). Emission spectra were separated using a linear unmixing algorithm providing separate grayscale images of each FP.

LSCM λ stacks acquired for all three cell lines, α7Yβ2C (Fig. 1, A and B), α7Y (C), and α4Yβ2C (D and E), revealed a reticulated pattern of subunit-associated fluorescence throughout much of the cytosolic region. This pattern strongly resembled the distribution of FP used to visualize the membranes of the endoplasmic reticulum (ER) (Grailhe et al., 2004) suggesting prominent ER localization of all three types of nAChR subunits. As expected, α4Y and β2C were colocalized. Likewise, α7Y and β2C colocalized (Supplemental Fig. S1).

FRET Demonstrates Coassembly of FP-Tagged nAChR α7 and β2 Subunits. To determine whether colocalized α7Y and β2C also were coassembled, FRET studies were conducted. Detection of FRET between FP-tagged α7 and β2 subunits would provide strong evidence of coassembly. Given that nAChR α4 and β2 subunits coassemble into heteropentameric receptors, and that we have shown FRET between fluorescently labeled subunits (Nashmi et al., 2003), the α4Yβ2C cell line was used as a positive control for FRET. As expected, FRET between CFP and YFP was observed in α4Yβ2C cells. It is noteworthy that FRET was also observed in α7Yβ2C cells and the reciprocally labeled α7Cβ2Y cells, revealing coassembly of FP-tagged α7 and β2 subunits (α7FP and β2FP, respectively). Moreover, FRET occurred at a level that implied that α7FP and β2FP subunits coassembled with efficiency comparable with that for α4Y and β2C subunits (Table 1).

Results from representative α4Yβ2C and α7Yβ2C cells show recovery of fluorescence intensity from the donor fluorophore, CFP, after photobleaching of the acceptor, YFP (Fig. 2). The y-axis (A and C) represents the normalized mean intensity of the FP (initial intensity before photobleaching set to 100%), and the x-axis is the bleach step where zero denotes the time before photobleaching. Each of the representative plots shows that CFP intensity increased as it was progressively dequenched by

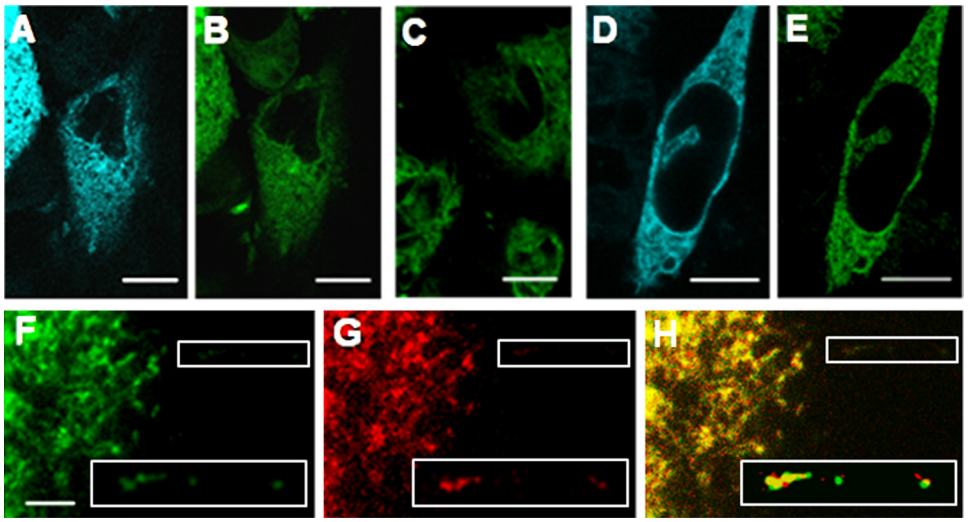

Fig. 1. LSCM confocal λ stack and TIRF images of cells illustrating distributions of fluorescently tagged nAChR subunits. Unmixed λ stack images of cells stably expressing one or more nAChR subunits (pseudocolored), as follows: β2C (A) and α7Y (B) (A and B in the same α7Yβ2C cell); α7Y (C) (in an α7Y cell); and β2C (D) and α4Y (E) (D and E in the same α4Yβ2C cell). A reticulated distribution of fluorescence was observed throughout the intracellular region, consistent with the distribution of the endoplasmic reticulum membrane (Grailhe et al., 2004). F to H, representative TIRF microscopy images (pseudocolored) of cell expressing α7Y (F, green) and β2Cherry (G, red) were merged to show colocalization (H, yellow) in the cell body as well as distal filopodia (box). Insets in F to H are enlarged views of boxed regions. Scale bars A to E, 10 μm; F to H, 5 μm.

TABLE 1
Mean FRET efficiency
Mean FRET efficiencies (E) for each combination of FP-tagged subunits. n refers to number of cells tested.

Cell ID	Subunit Combination		Mean E ± S.E.M.	n
α7Yβ2C	α7-YFP	β2-CFP	23.3 ± 1.8	8
α7Cβ2Y	α7-CFP	β2-YFP	34.6 ± 3.5	12
α4Yβ2C	α4-YFP	β2-CFP	27.9 ± 1.6	16
α7Y-GCβC	α7-YFP	GCβ-CFP	−2.7 ± 2.3	7
α7C-GCαY	α7-CFP	GCα-YFP	−4.9 ± 2.2	5
β2C-GCαY	β2-CFP	GCα-YFP	−1.5 ± 2.2	9
GCαY-GCβC	GCα-YFP	GCβ-CFP	24.5 ± 3.0	6

the stepwise photodestruction of YFP. To compare the relative levels of coassembled subunits, FRET efficiency (the efficiency of energy transfer from CFP to YFP: $E = [1 - (I_{DA}/I_D)] \times 100\%$) was calculated. E was determined for each cell tested using scatter plots (as in Fig. 2, B and D) of the increase in CFP (recovery) versus the decrease in YFP intensity (bleaching) to extrapolate I_D. Both scatter plots had positive slopes, again indicating FRET (Nashmi et al., 2003) between FP-tagged β2 subunits and either YFP-tagged α4 or α7 subunits. FRET was also observed in α7Cβ2Y cells in which the α7 and β2 subunits were reciprocally labeled (Table 1).

To rule out FRET from casual contact between FP-tagged subunits, FP-tagged GluCl subunits (Slimko and Lester, 2003) were used for negative control experiments. nAChR subunits usually do not coassemble with GluCl subunits (Nashmi et al., 2003; Drenan et al., 2008), even though all of these subunits are members of the Cys-loop receptor family (Lester et al., 2004). For each GluCl subunit, the FP was fused into the intracellular domain (Slimko and Lester, 2003) analogous to the C2 loop FP fusions in our FP-tagged nAChR subunits. The YFP-tagged GluCl α subunit (GCαY) was transiently coexpressed with the nAChR β2C fusion protein, providing one set of negative controls (representative β2C-GCαY cell; Fig. 2, E and F). For a second negative control, a CFP-tagged GluCl β subunit (GCβC) was transiently coexpressed in the α7Y cell line (α7Y-GCβC cells; Table 1). A third negative control involved transient coexpression of GCαY in the α7C cell line (α7C-GCαY cells; Table 1). As expected, FRET did not occur in any of the negative control cells. To rule out the possibility that the lack of FRET was due to FP insertions in GluCl subunits hindering subunit coassembly, GCαY and GCβC were transiently coexpressed (Nashmi et al., 2003; Drenan et al., 2008) in SH-EP1 cells. FRET occurred in GCαY-GCβC cells (Fig. 2, G and H) with E similar to values for α7Yβ2C and α4Yβ2C cells (Table 1), indicating that the GluCl subunit-FP fusions did not impede the potential for coassembly. Thus, the FRET we observed between FP-tagged α7 and β2 nAChR subunits resulted from specific coassembly.

As stated above, E provides a means to compare the efficiency of coassembly from the pool of FP-tagged subunits. Mean values of E were calculated for each combination of

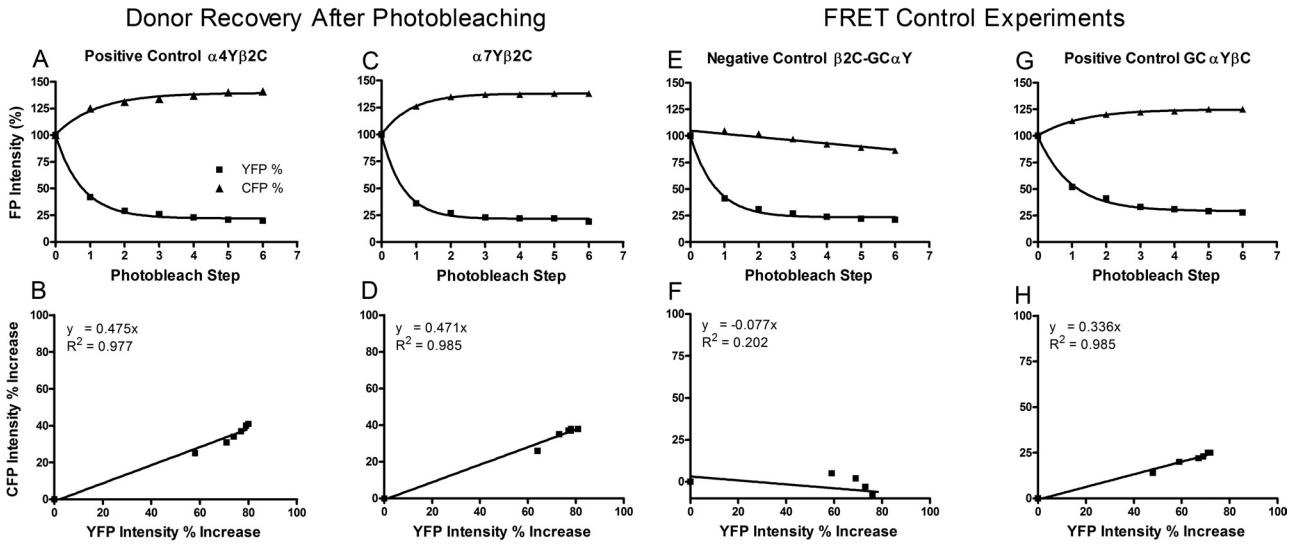

Fig. 2. FRET between YFP- and CFP-labeled nAChR subunits. A and B, FRET between YFP and CFP in a representative, positive control, α4Yβ2C cell indicated coassembly of α4Y and β2C subunits in heteromeric receptors, as expected. A, increase in fluorescence intensity of CFP (▲) and decrease in YFP fluorescence intensity (■) as YFP was photobleached and CFP was dequenched (*y*-axis; 100% represents the normalized intensity before photobleaching). The *x*-axis designates the bleach step with zero indicating the initial intensity measurement for each fluorophore before photobleaching. B, scatter plot of the increase in CFP intensity (recovery; *y*-axis) versus the decrease in YFP intensity (bleaching; *x*-axis) expressed as percentage change from the initial value of 100%. The slope was used to calculate I_D, the intensity of CFP in the absence of the acceptor, which was then used to determine FRET efficiency ($E = [1 - (I_{DA}/I_D)] \times 100\%$). C and D, FRET in a representative α7Yβ2C cell was observed between the two FP-tagged subunits, α7Y and β2C, indicating coassembly as heteromeric nAChRs. C, CFP (▲) fluorescence intensity increased as YFP (■) was photobleached (axes as in A). D, scatter plot used to determine I_D (axes as in B). F to I, negative and positive controls using GluCl channel subunits. E and F, negative control cells were cotransfected with a fluorescently tagged nAChR subunit (α7Y, α7C, or β2C) and a fluorescently tagged glutamate-gated chloride channel subunit (GCαY or GCβC). E, representative plot of fluorescence intensity (*y*-axis as in A) as a function of photobleaching step (*x*-axis) for a negative control cell expressing β2C and GCαY, which do not coassemble. As YFP (■) was bleached, CFP (▲) fluorescence intensity did not increase, indicating that FRET did not occur and thus that the two subunits did not coassemble (i.e., no significant FRET results from casual contact between unassembled, mismatched FP-labeled subunits). F, plot of changes in CFP fluorescence intensity increase (*y*-axis as in B) as a function of YFP fluorescence intensity decrease (*x*-axis). The small, negative slope yields a negative value for FRET efficiency, consistent with only modest photobleaching of CFP during photodestruction of YFP. G and H, FRET occurs between GCαY and GCβC subunits in a representative, positive control cell. G, CFP (▲) dequenching occurred as YFP (■) was photobleached (*y*-axis as in A), indicating coassembly of GCαY and GCβC subunits. H, there is a positive correlation (positive slope) between the percentage increase in CFP fluorescence (*y*-axis as in B) as YFP fluorescence decreases that is due to photobleaching, indicating FRET between GCαY and GCβC subunits and confirming that FP insertions did not prevent coassembly.

subunits described above (summarized in Table 1). Values of E for positive control cell lines α4Yβ2C and GCαY-GCβC were consistent with published reports on coassembly propensity for compatible Cys-loop receptor subunits (Nashmi et al., 2003; Drenan et al., 2008). Consistent with a lack of FRET, mean E values for all three negative control subunit combinations were indistinguishable from zero.

In stark contrast to subunits that do not coassemble, E values for α7Yβ2C cells and α7Cβ2Y cells were 23.3 ± 1.8 and 34.6 ± 3.5, respectively, which suggest relatively efficient coassembly of the two FP-subunits. In addition, this directionality further supports coassembly, because if FRET could occur from casual contact, it would result in similar efficiencies. Moreover, differences between the mean E values for complementarily labeled α7Yβ2C cells and α7Cβ2Y cells were significant ($p = 0.02$) suggesting that the higher mean E for α7Cβ2Y cells was due to a greater proportion of subunits tagged with the acceptor YFP. This is consistent with the idea that a greater number of β2 subunits may have been present in α7β2 assemblies. Thus, not only do FP-tagged α7 and β2 subunits coassemble with efficiency similar to that of FP-tagged α4 and β2 subunits in SH-EP1 cells, but the differences in E between the two reciprocally labeled FP-subunit combinations may reveal β2 subunit-predominant coassembly with α7, at least in our cell line.

TIRF Microscopy Reveals that FP-Tagged α7 and β2 Subunits Are Coassembled in Cell Surface Regions. TIRF microscopy was used to determine whether coassembled FP-tagged α7 and β2 subunits localized to the plasma membrane of SH-EP1 cells. TIRF, as used in these studies, captures fluorescence emissions emanating from an evanescent wave that extends within ~100 nm above the coverslip. This region includes the plasma membrane of cells adhering to the coverslip as well as the intracellular region near the plasma membrane. Thus, FP-tagged nAChR subunits appearing in the images might be expressed in the plasma membrane, where they could contribute to function. On the other hand, they may be located in intracellular regions near the membrane, where they would not so contribute. To minimize ambiguity, long, narrow membrane protrusions devoid of ER were used to identify regions of the plasma membrane. These included distal regions of filopodia-like structures and smaller micropodia-like protrusions (Grailhe et al., 2004) that were not directly located under the cell body. These processes were rendered visible by localization of FP-tagged subunits (Fig. 1, F and G). We traced regions of interest (ROI) around these structures for comparing levels of expression in the plasma membrane region versus the cell body.

To obtain a measurement for comparing levels of plasma membrane expression between cells, the adjusted mean intensity (mean intensity minus background) of an ROI was normalized to the adjusted mean intensity of its cell body (Grailhe et al., 2004). Using this normalized fluorescence intensity (I_n), we compared plasma membrane expression levels of FP-tagged subunits labeled with YFP or with mCherry FP. Our TIRF system was unable to excite CFP, so we were not able to calculate the I_n for subunits labeled with CFP. We measured the I_n of α7Y, α4Y, and/or β2-mCherry FP (β2Ch) in cells expressing α7Y alone, α7Y with β2FP (β2C or β2Ch), or α4Y with β2C. Coexpression of β2FP did not affect relative levels of α7Y observed in the plasma membrane because no significant difference was found between the I_n for YFP fluorescence in cells expressing α7Y and β2FP versus α7Y alone. For YFP, I_n was 0.44 ± 0.02 (mean ± S.E.M., n = 86) for ROIs of cells expressing α7Y alone and 0.40 ± 0.05 (n = 41) for those in cells expressing α7Y and β2FP (p = 0.38). On the other hand, plasma membrane localization was significantly higher for α4Y coexpressed with β2C (for YFP, I_n was 0.79 ± 0.05, n = 55) than for α7Y, regardless of whether α7Y was singly expressed or coexpressed with β2FP ($p < 0.0001$ each).

For cells coexpressing α7Y and β2Ch, both FPs could be visualized using our TIRF system. The I_n derived from mCherry FP was calculated for the same plasma membrane ROIs used for measuring I_n of α7Y. No significant difference was found between the I_n values derived from α7Y and β2Ch ($p = 0.86$, $n = 28$). Thus, both α7Y and β2Ch were expressed in plasma membrane processes in the same proportion relative to their expression in the cell body. Furthermore, the mean intensity of YFP in the cell body region derived from α7Y subunits did not change when β2FP subunits were coexpressed ($p = 0.90$), suggesting that the expression level of α7 subunits was not altered by coexpression of β2 subunits. Moreover, both subunits were colocalized. Pseudocolored images of a cell with filopodia (Fig. 1, F and G) show the YFP channel (green; F) and the mCherry FP channel (red; G) overlaid to reveal α7Y and β2Ch colocalization in both the ER-like region of the cell body (yellow; H) and also in filopodia (inset; H). Colocalization in the plasma membrane region implied that α7Y and β2Ch coassembled as pentameric proteins (Keller et al., 2001).

The chaperone protein RIC-3 has been reported to facilitate expression of functional α7 nAChRs (Halevi et al., 2003). We transfected α7Yβ2C, α7Y and α7 cells with RIC-3 cDNA to study the effect of the chaperone on plasma membrane localization and function of heteropentameric receptors formed by these two subunits. It is noteworthy that in two separate experiments, localization of fluorescence in membrane processes resembling filopodia could not be detected in α7Yβ2Ch cells coexpressing RIC-3. In contrast, no such reduction in fluorescence in plasma membrane processes was observed in α7Y cells coexpressing RIC-3. Upon examination of TIRF images of α7Yβ2Ch/RIC-3 cells (n = 16), only one membrane process in one cell had fluorescence above background levels. A few cells exhibited fluorescence corresponding to α7Y and β2Ch in structures resembling micropodia beneath cell bodies. However, these structures were in cell body regions that had mean fluorescence intensities for YFP and mCherry FP at levels similar to α7Yβ2Ch cells without RIC-3. Thus, the possibility that they reflected ER expression made these structures ambiguous indicators of cell surface localization, and they could not be used to measure such. Mean fluorescence intensities from α7Y and β2Ch in the cell body region of α7Yβ2Ch cells versus α7Yβ2Ch/RIC-3 cells were not statistically different from each other ($p = 0.56$ and 0.34 for α7Y and β2Ch, respectively). Furthermore, the two subunits were colocalized in the cell body region regardless of RIC-3 coexpression. This suggests that synthesis and coassembly of the intracellular tagged subunits was not significantly altered by RIC-3 coexpression, yet trafficking to filopodia-like processes was sharply reduced. Altered trafficking was not unexpected because varied effects on nAChR traf-

ficking with RIC-3 coexpression have been reported (Halevi et al., 2003; Lansdell et al., 2005).

Subunit Coassembly and Receptor Pharmacology Probed with Mutant Subunits

Gain of Function α7and β2 Subunits Coassemble into Functional Receptors. As another means to examine the assembly of β2 into α7 nAChR complexes, we took advantage of the gain-of-function L9′T mutants as pharmacological reporters. Previous work has shown that mutation of the Leu9′ residue into a Thr causes profound modification of human α7 nAChR properties (Revah et al., 1991; Bertrand et al., 1992). The pleiotropic modifications brought by this mutation include the loss of desensitization and conversion of some competitive antagonists into agonists (Bertrand et al., 1992). Typical effects caused by the L9′T mutation include agonist activity by the competitive inhibitor, dihydro-β-erythroidine (DHβE) at $\alpha7^{L9'T}$ nAChRs, yet DHβE has no effect at wild-type α7 nAChRs (Fig. 3A). Coexpression of $\alpha7^{L9'T}$ with β2 subunits in oocytes yielded a significant reduction of the DHβE agonistic activity (Fig. 3, A and B). Moreover, and as expected if β2 subunits are incorporated into the receptor, recovery of DHβE agonism was observed upon coexpression of $\alpha7^{L9'T}$ with $\beta2^{L9'T}$ subunits.

In addition, a gain-of-function mutation for mouse β2 subunits ($m\beta2^{V9'S}$) was expressed in oocytes with mα7-YFP subunits (derived from the α7Y construct used in the FRET and TIRF experiments). Several significant differences in ACh-evoked current were noted when mα7-YFP subunits were coexpressed with $m\beta2^{V9'S}$ subunits compared with mα7-YFP subunits expressed alone. When expressed at a 1:10 ratio of mα7-YFP to $m\beta2^{V9'S}$ subunits, ACh concentration-response curves shifted to the right (Fig. 4A), and EC_{50} values increased (Supplemental Table S2). On the other hand, no

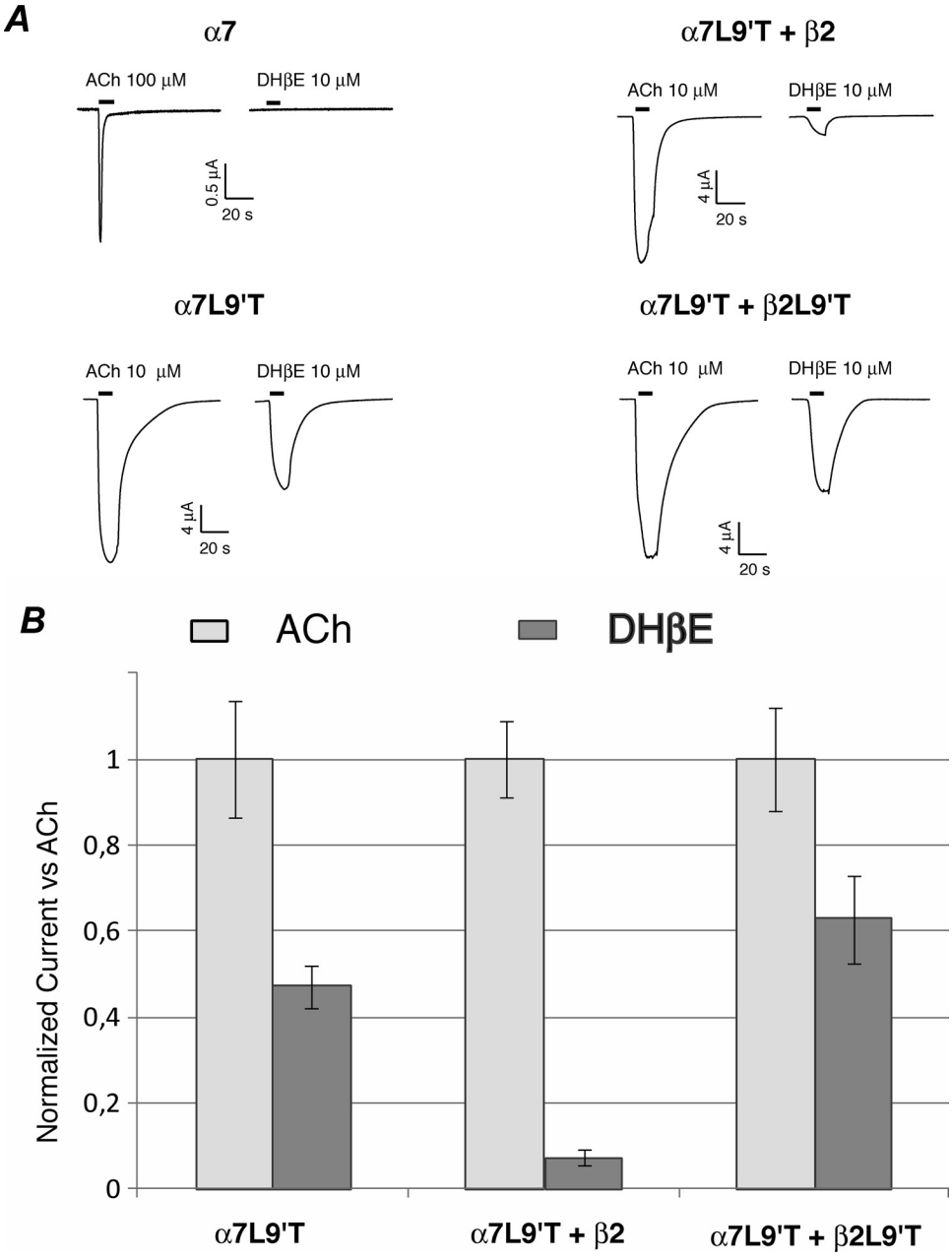

Fig. 3. Incorporation of β2 subunits into the α7 nAChR complex. Human wild-type and gain-of-function mutant subunits expressed in *X. laevis* oocytes. A, typical whole-cell current response time courses observed in oocytes expressing wild-type α7, $\alpha7^{L9'T}$, $\alpha7^{L9'T}$ + β2, or $\alpha7^{L9'T}$ + $\beta2^{L9'T}$ subunits (1:1 injection ratio for coexpression). B, peak inward currents measured in a series of cells ($n \geq 4$) in response to ACh and DHβE. Currents were normalized versus ACh. DHβE has no agonistic effect for wild-type α7 nAChRs, yet it does evoke current from $\alpha7^{L9'T}$ nAChRs. Both effects are as expected. It is noteworthy that expression of the β2 subunit causes a significant reduction of the DHβE-evoked current. Conversely, expression of the $\beta2^{L9'T}$ subunit rescues the agonist effect of DHβE.

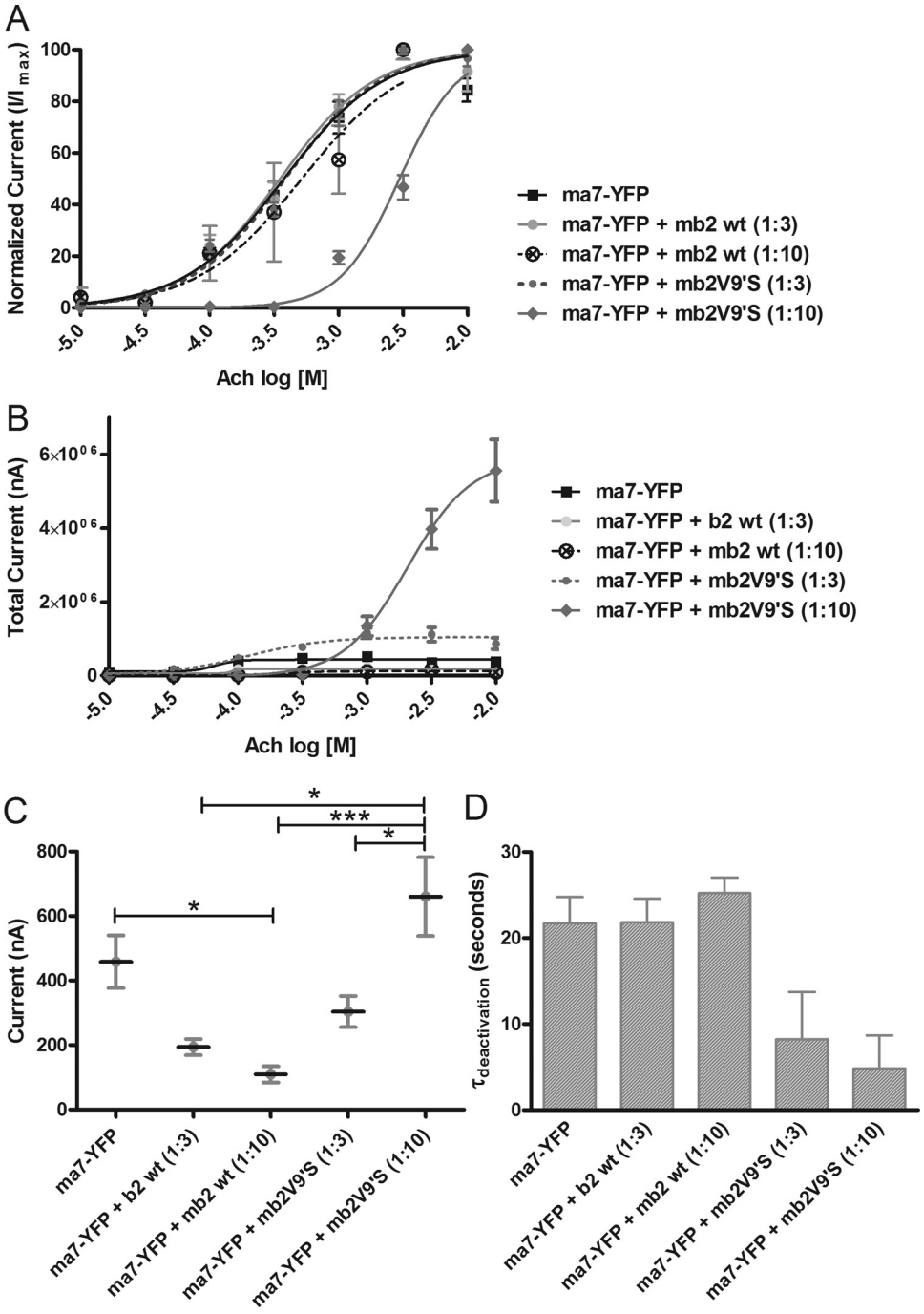

Fig. 4. Effects of coexpression of mβ2 or m$\beta2^{V9'S}$ gain-of-function mutant subunits, expressed in *X. laevis* oocytes, on responses to ACh (mα7-YFP to β2 subunit ratios were 1:3 and 1:10). A, relationship of normalized current to ACh concentration. Responses for mα7-YFP subunits expressed alone versus mα7-YFP coexpressed with m$\beta2^{V9'S}$ subunits at a 1:10 ratio were significantly different as determined by a nonlinear fit ($p < 0.05$; GraphPad Prism). B, integrated (total) current. The differences in response between mα7-YFP subunits expressed alone and mα7-YFP coexpressed with m$\beta2^{V9'S}$ subunits were statistically significant for expression at 1:3 and 1:10 ratios ($p < 0.05$ and < 0.001, respectively). C, peak current in response to 3 mM ACh (*, $p < 0.05$; ***, $p < 0.001$). D, rate of deactivation ($\tau_{deactivation}$) after application of 3 mM ACh. Differences in mean values of $\tau_{deactivation}$ for mα7-YFP and mα7-YFP subunits coexpressed with wild-type mβ2 subunits (1:3 or 1:10) were not statistically significant. However, mα7-YFP coexpressed with m$\beta2^{V9'S}$ subunits did result in significantly lower rates ($p < 0.05$ and $p < 0.001$ for a 1:3 and 1:10 expression ratio, respectively). ($n = 6-8$ oocytes per group.).

differences in ACh concentration-response curves and EC_{50} values were noted when mα7-YFP subunits were expressed at a 1:3 ratio with m$\beta2^{V9'S}$ subunits relative to when mα7-YFP subunits were expressed alone. In addition, coexpression of mα7-YFP with m$\beta2^{V9'S}$ subunits at 1:3 and 1:10 injection ratios resulted in significant increases in peak current amplitudes compared with those seen upon coexpression of mα7-YFP with wild-type mβ2 subunits at both injection ratios (Fig. 4C). Likewise, when mα7-YFP and m$\beta2^{V9'S}$ subunits were coexpressed, the total (integrated) charge in response to higher concentrations of ACh was significantly higher than when mα7-YFP subunits were expressed alone (Fig. 4B). This effect was greater when mα7-YFP and m$\beta2^{V9'S}$ subunits were coinjected at a 1:10 ratio ($p < 0.001$) than at a 1:3 ratio ($p < 0.05$). Coexpression of wild-type mα7 with mβ2 or m$\beta2^{V9'S}$ subunits produced similar responses to those noted above (Supplemental Fig. S4; Supplemental Table S2). In addition, coexpression of m$\beta2^{V9'S}$ with mα7-YFP subunits at either ratio markedly decreased the rate of deactivation ($p < 0.05$ and < 0.001 for 1:3 and 1:10, respectively; Fig. 4D). On the other hand, coexpression of wild-type mβ2 with mα7-YFP subunits had no significant effect on this rate for either the 1:3 or 1:10 injection ratio ($p > 0.05$). Taken together, the changes in ligand sensitivity, evoked current amplitudes, and rate of deactivation upon coexpression of human or mouse gain-of-function β2 subunits with α7 subunits confirms that these β2 subunits incorporated into functional receptors.

TABLE 2

Responses to agonists

Agonist-evoked responses in oocytes injected with wild-type or human nAChR subunits are shown for several agonists (mean ± S.E.M.).

Oocytes were injected with α7 subunits alone, or with α7 and β2 subunits at a 1:1 ratio. *n* refers to number of oocytes. Normalized I_{max} for α7β2 was calculated for a compound by dividing the mean maximum current (I_{max}) recorded from oocytes expressing α7β2 by the I_{max} of cells expressing α7 receptors exposed to the same compound. Likewise, I_{max} for α7-expressing cells was divided by itself, such that the normalized I_{max} = 1 for each compound.

Agonist and Subunit(s)	*n*	Normalized I_{max}			EC_{50}		
		Mean	S.E.M.	*p*	Mean	S.E.M.	*p*
					μM	*μM*	
Acetylcholine (1280 μM[a])							
α7	6	1.00	1.22	0.72	140.67	7.22	0.87
α7β2	7	0.86	0.75		136.71	5.82	
Choline (1280 μM[a])							
α7	16	1.00	0.13	0.02	1.77	0.23	0.42
α7β2	12	0.55	0.05		2.00	0.18	
Carbachol (3200 μM[a])							
α7	13	1.00	0.46	0.04	339.69	6.77	0.57
α7β2	21	0.63	0.12		361.76	6.40	
Epibatidine (10 μM[a])							
α7	9	1.00	0.15	0.002	1.17	0.18	0.01
α7β2	8	0.47	0.20		2.25	0.27	
PNU-282987 (40 μM[a])							
α7	7	1.00	0.17	0.17	2.11	0.12	< 0.001
α7β2	6	1.12	0.31		4.37	0.21	

[a] Agonist concentrations used to measure I_{max}.

β2 Subunit Incorporation into nAChRs also Containing α7 Subunits Results in a Reduction of Evoked Current Amplitudes without Substantial Alterations in Ligand Concentration-Response Curves. A reduction in agonist-evoked current amplitudes of up to ~2-fold was observed when human β2 subunits were coexpressed with α7 subunits (1:1 ratio) in oocytes. This occurred for several compounds, including choline, carbachol. and epibatidine, but not for ACh or the α7-selective agonist *N*-(3*R*)-1-azabicyclo[2.2.2]oct-3-yl-4-chlorobenzamide (PNU-282987) (Table 2, Normalized I_{max}). In addition, we observed a significant reduction in ACh-evoked current amplitudes when mα7-YFP subunits were coexpressed with wild-type mβ2 subunits at a 1:10 ratio ($p < 0.01$) compared with when mα7-YFP subunits were expressed alone. When there was a 1:3 ratio for expression of mα7-YFP:mβ2 subunits, a trend toward lower current was noted, but no significant difference was found after adjustment for multiple comparisons (Fig. 4C). Likewise, a 2-fold reduction in peak whole-cell current elicited by choline was also noted in SH-EP1 cells expressing fluorescently tagged mouse α7Yβ2C nAChRs compared with when α7 or α7Y nAChRs were expressed (Table 3; Supplemental Fig. S2).

Most surprising were the comparable and sometimes nearly identical concentration-response curves and EC_{50} values for α7 subunit expression alone versus α7 and β2 subunit coexpression. These similarities persisted over the range of subunit species type and expression systems we employed, and they were irrespective of whether or not the subunit was fluorescently labeled. For example, concentration-response curves for choline-evoked current were markedly similar for SH-EP1 cells expressing mouse α7 nAChRs, α7Y nAChRs, or α7Yβ2C nAChRs (Supplemental Fig. S3A). Yet, there were differences in the Hill slopes, which were 1.63 ± 0.13, 1.41 ± 0.09, and 1.15 ± 0.13 (mean ± S.E.M., $n = 7$) for α7/RIC-3, α7Y/RIC-3, and α7Yβ2C/RIC-3 cells, respectively. However, the only significant difference was between α7Yβ2C/RIC-3 and α7/RIC-3 cells ($p = 0.020$). Likewise, concentration-responses curves for inhibition of choline-induced current by MLA were nearly matched for the three cell lines (Supplemental Fig. S3B). Hill slopes for α7/RIC-3, α7Y/RIC-3, and α7Yβ2C/RIC-3 cells were 0.96 ± 0.09, 1.05 ± 0.09, and 1.48 ± 0.12 (mean ± S.E.M., $n = 7$), respectively. Both α7/RIC-3 and α7Y/RIC-3 cells had significantly lower slopes than α7Yβ2C/RIC-3 cells ($p = 0.005$ and 0.015, respectively). Likewise, for mouse subunits expressed in oocytes, choline concentration-response curves were comparable whether mα7-YFP or mα7 subunits were expressed alone or along with mβ2 subunits (1:3 or 1:10 ratios; Fig. 4; Supplemental Fig. S4), yielding similar EC_{50} values (Supplemental Table S2). For cells having a 1:10 ratio of either mα7-WT or mα7-YFP to mβ2, we again observed a reduction in the Hill slope compared with cells expressing only the α7 subunit. It is noteworthy that when human α7 and β2 subunits were coexpressed in oocytes at a 1:1 ratio, no significant differences were observed for the apparent sensitivities to ACh, choline, or carbachol (Table 2, EC_{50}), whereas there was a decrease in sensitivity to epibatidine and PNU-282987. However, as shown in Fig. 5A, coexpression with the β2 subunit at a 1:10 ratio (α7:β2) caused no apparent differences in the concentration-response relationship for the positive allosteric modulator PNU-120596. Furthermore, only a small difference was observed in sensitivity to the competitive inhibitor MLA in oocytes expressing α7 subunits alone or in combination with β2 subunits (Fig. 5B). Overall, these data show several, striking similarities in sensitivities to common pharmacological agents between cells expressing α7 subunits alone or expressing both α7 and

TABLE 3

Whole-cell current in SH-EP1 cells

Whole-cell mean peak current in response to 10 mM choline (mean ± S.E.M; $n = 7$ cells each). Cells were transfected with mouse subunits, with or without transfection of RIC-3.

Cell Line Description	Peak Current
	pA
α7	205 ± 26
α7/RIC-3	510 ± 48
α7Y	178 ± 19
α7Y/RIC-3	498 ± 54
α7Yβ2C	108 ± 23
α7Yβ2C/RIC-3	220 ± 29

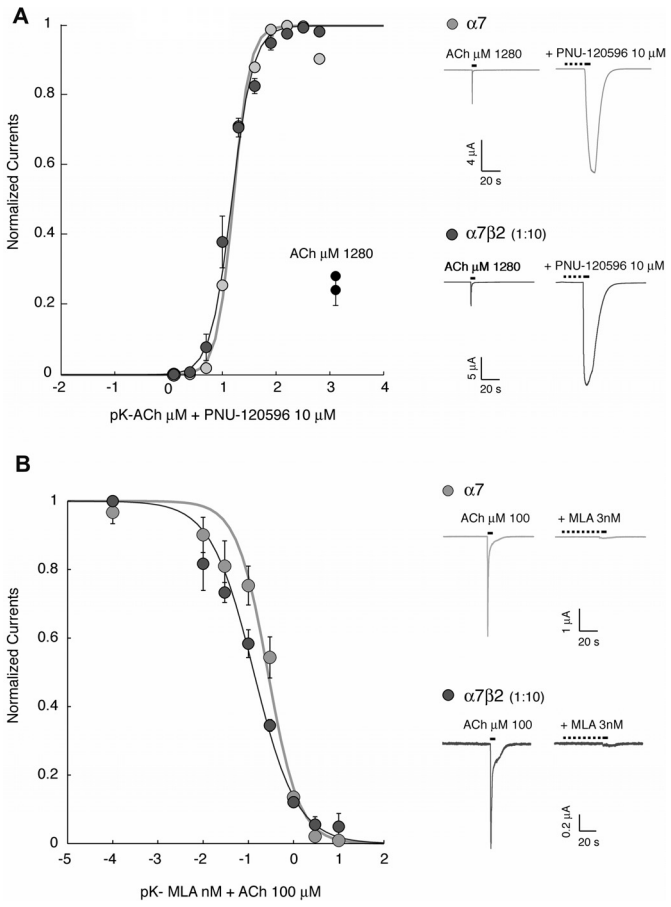

Fig. 5. Expression of $\beta 2$ subunits does not modify the pharmacological properties of $\alpha 7$ nAChRs. A, effects of the positive allosteric modulator PNU-120596 were assessed in oocytes expressing $\alpha 7$ subunits alone or $\alpha 7$ and $\beta 2$ subunits injected at a 1:10 ratio. Concentration-response curves, determined before and after PNU-120596 treatment, reveal no detectable differences between oocytes expressing $\alpha 7$ or $\alpha 7$ plus $\beta 2$ subunits ($n \geq 5$). Continuous lines through the data points are the best fits obtained with the empirical Hill equation. Currents were normalized versus the control response evoked by 1280 μM ACh. Typical ACh-evoked currents recorded before and after PNU-120596 exposure are shown to the right. B, effects of the competitive inhibitor MLA. Plot of the peak inward current evoked by a constant ACh test pulse (100 μM) for different MLA concentrations yielded a typical concentration-inhibition curve that is readily fitted by the Hill equation (IC_{50} = 0.27 nM; n_H = 1.3, n = 5 for $\alpha 7$ nAChRs and IC_{50} = 0.13; n_H = 0.9, n = 4 for $\alpha 7\beta 2$ nAChRs). Expression of the $\beta 2$ subunit might yield a small increase in MLA sensitivity. Typical ACh-evoked currents recorded before MLA exposures (45 s) are shown to the right.

$\beta 2$ subunits. Only a few compounds exhibited relatively modest differences between homomeric versus heteromeric $\alpha 7$ receptors. In contrast, a clear difference in the inhibition of ACh-evoked current by the antagonist DHβE was observed between $\alpha 7$ and $\alpha 7\beta 2$ receptors.

Incorporation of $\beta 2$ Subunits into $\alpha 7$ nAChRs Results in Sensitivity to Low Concentrations of DHβE. DHβE, a competitive antagonist, is known to discriminate between the $\alpha 4\beta 2$ and $\alpha 7$ nAChRs with a difference in IC_{50} of 0.1 versus 20 μM for these two receptors, respectively (Chavez-Noriega et al., 1997). In addition, Liu et al. (2009) employed DHβE to probe pharmacological differences between cells containing $\alpha 7$ nAChRs in the ventral tegmental area and cells in the MS/DB expressing putative $\alpha 7\beta 2$-containing receptors in which the latter displayed a ~500-fold higher sensitivity to inhibition of choline-induced current by DHβE (IC_{50} = 0.17 μm). We reasoned that if $\alpha 7$ and $\beta 2$ subunits were coassembled into functional receptors, these heteromeric receptors would also display similar sensitivity to DHβE inhibition. Experiments were carried out in sibling oocytes injected either with $\alpha 7$ or with $\alpha 7$ and $\beta 2$ in a 1:10 ratio; to minimize experimental differences, the $\alpha 7$ concentration was identical and measurements were effectuated on the same day with the same solutions.

In agreement with published data on $\alpha 4\beta 2$, exposure to DHβE caused inhibition of ACh-induced current (200 μM, 5 s) in a dose-dependent manner. Although DHβE inhibited both the $\alpha 7$ and $\alpha 7\beta 2$ nAChRs, a difference was observed in the low concentration range (Fig. 6). Although the concentration inhibition curve at the $\alpha 7$ nAChRs displayed a smooth profile, and data were readily fitted by a single Hill equation with an IC_{50} at 4.58 $\pm$ 0.4 μM and n_H of 1.2 $\pm$ 0.1 (n = 7), data obtained with $\alpha 7\beta 2$ were best fitted using a dual Hill equation with an IC_{50} of 0.09 $\pm$ 0.04 μM and n_H of 0.9 $\pm$ 0.16 for the high-affinity component and an IC_{50} of 5.91 $\pm$ 0.8 and n_H of 1.7 $\pm$ 0.2 (n = 7) for the low-affinity component. The high-affinity component represented a fraction of 23 $\pm$ 4% of the overall current. Responses were normalized to unity for the current evoked in the absence of antagonist and the mean current was 1.8 $\pm$ 0.2 μA in cells expressing $\alpha 7$ receptors and 1.03 $\pm$ 0.25 μA for cells expressing $\alpha 7\beta 2$ receptors.

In contrast, the degree of inhibition of ACh-evoked current by DHβE in the present study was much less than inhibition of choline-evoked current by DHβE in rodent MS/DB cells expressing putative $\alpha 7\beta 2$ nAChRs (Liu et al., 2009). However, when Liu et al. (2009) coexpressed rat $\alpha 7$ and $\beta 2$ subunits in oocytes, they also reported less inhibition (Supplemental Figures). A reduction in inhibition by DHβE is consistent with an admixture of $(\alpha 7)_5$ and $(\alpha 7)_m(\beta 2)_n$ nAChRs. Because both groups observed a reduction in efficacy when subunits were expressed in oocytes, compared with natively expressed receptors, this suggests that native cellular mechanisms in the rodent MS/DB favored coassembly of heteromeric receptors and that these mechanisms are lacking in oocytes. The additional reduction in the effect of DHβE in the present study versus the responses in oocytes reported by Liu et al. (2009) may be attributed to differences in agonists, oocytes, and species of receptor subunits.

Probe of Binding Sites Using Cysteine Mutants. To determine whether the $\alpha 7$-$\beta 2$ subunit interfaces contribute functional binding sites for ACh, we coexpressed human $\alpha 7$ and $\beta 2$ subunits with our previously described (Papke et al., 2011) cysteine mutant in one subunit or the other (L119C in $\alpha 7$ and L121C in $\beta 2$). We previously showed that when these mutations are present in the complementary face of an agonist binding site, exposure to a cationic sulfhydryl reagent, such as MTSEA, results in a covalent modification that prevents the application of ACh or other agonists from activating the receptors. We injected RNA at a 1:4 ratio of $\alpha 7$ to $\beta 2$ subunits, both with and without coinjection of RIC-3.

Two initial control responses to 300 μM ACh were obtained from all cells, and the average peak current and net charge of these responses were used to normalize the data for each cell. Consistent with our other observations, the main effect of $\beta 2$ subunit coexpression was an overall reduction in ACh-evoked currents compared with our typical responses with $\alpha 7$ subunits injected alone. This effect was somewhat less in the cells coinjected with RIC-3. After measuring the preapplica-

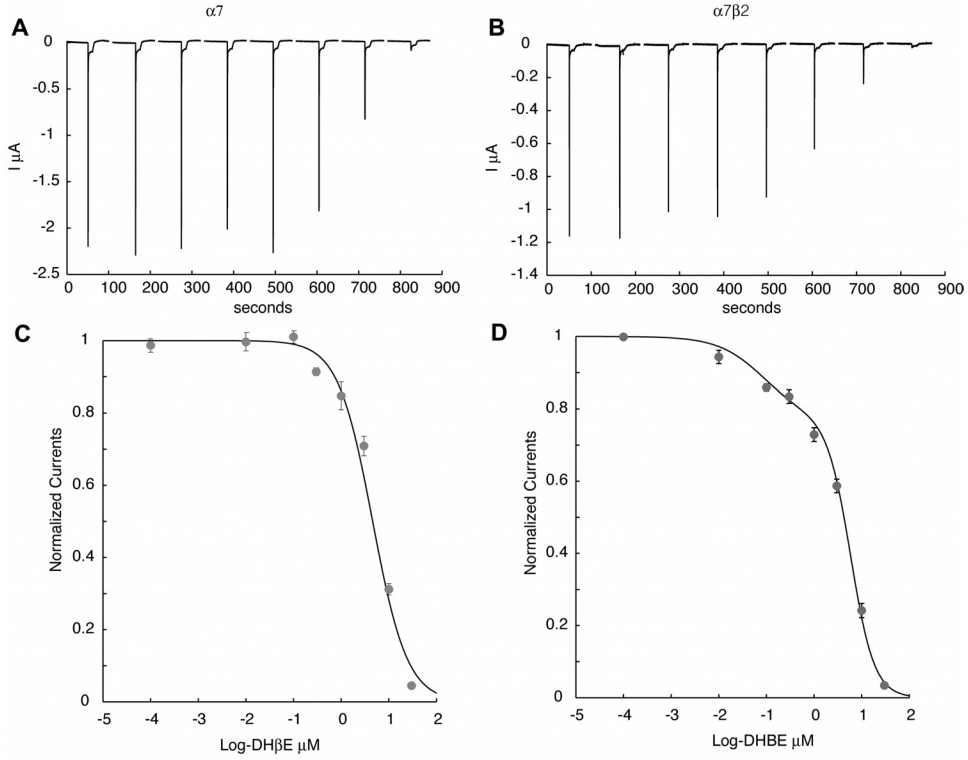

Fig. 6. DHβE application differentially inhibited ACh-induced current in α7β2 versus α7 nAChRs. Mean current evoked by ACh (200 μM, 5 s), in the absence of antagonist, for cells expressing α7 receptors was 1.8 ± 0.2 μA and 1.03 ± 0.25 μA for cells expressing α7β2 receptors. Sample traces for cells expressing α7 and α7β2 are shown in A and B, respectively. DHβE inhibited current in a dose–dependent manner. The concentration inhibition curve for α7 nAChRs displayed a smooth profile (C) with an IC_{50} of 4.58 ± 0.4 μM and n_H of 1.2 ± 0.1 (n = 7). In contrast, the response of α7β2 nAChRs were best fit with a dual Hill equation (D) with an IC_{50} of 0.09 ± 0.04 μM and n_H of 0.9 ± 0.16 for the high-affinity component and an IC_{50} of 5.91 ± 0.8 and n_H of 1.7 ± 0.2 (n = 7) for the low-affinity component. Responses were normalized to the current evoked in absence of antagonist.

tion control responses, cells were treated with 2 mM MTSEA for 5 min and then stimulated again with 300 μM ACh. The post treatment responses were compared with the control ACh responses immediately preceding the MTSEA. There were no significant effects of MTSEA treatment on either peak current or net charge responses of cells coinjected with α7 subunits and $\beta2^{L121C}$ mutant subunits (Fig. 7; p values ranged from 0.25 to 0.61, n values were 12 for cells without RIC-3, and 13 for cells injected with RIC-3).

Selective knockout of the binding sites involving β2 subunits ($\beta2^{L121C}$ mutant) revealed that α7-β2 subunit interfaces do not bind ACh in a manner that leads to channel activation. This implies that only receptors with adjacent α7-α7 subunits could bind agonists productively. Receptors with a single α7-α7 interface might respond; receptors with several such interfaces would probably respond more readily (Williams et al., 2011).

Discussion

Our principal findings are that FP-tagged nAChR α7 and β2 subunits coassemble and are trafficked to the plasma membrane, where they function, and that coexpression of β2 with α7 subunits causes a significant decrease in agonist-evoked whole-cell current amplitudes. It is noteworthy that this decrease occurs without affecting the concentration-response characteristics of some common agonists and antagonists, which may partially explain why it has been so difficult to unambiguously identify α7β2 nAChRs in vivo. Moreover, and for the first time, we show that the α7-β2 interface does not bind ligand in a functionally productive manner. This presumably leaves only the α7-α7 interface(s) to translate binding of agonist into channel opening, thus explaining both the lower peak current responses for α7β2 nAChRs relative to α7 nAChRs and the similar ligand sensitivities for α7 nAChRs and α7β2 nAChRs observed in our study.

FRET and TIRF Microscopy of Fluorescently Tagged Subunits Reveals Coassembly of α7 and β2 Subunits and Plasma Membrane Localization

FRET Reveals FP-Tagged nAChR α7 and β2 Subunits Coassemble in Mammalian Cells. Fluorescently tagged mouse α7 and β2 subunits (α7FP and β2FP, respectively) were expressed in mammalian SH-EP1 cells. LSCM confirmed that α7FP and β2FP subunits colocalize, and FRET experiments revealed that they coassemble with efficiency resembling that of α4 and β2 subunits, known to form functional α4β2 nAChRs. It is noteworthy that the FRET efficiency for α7C-β2Y coassembly was significantly higher (34.6%) than for the reciprocally labeled α7Y-β2C coassembly (23.3%). This mirrors findings from α4FP and β2FP coassembly (E = 34 and 24% for α4C-β2Y and α4Y-β2C, respectively; Khakh et al., 2005), suggesting that receptors contained more β2 than α4 subunits. Thus, it is likely that more β2 subunits than α7 subunits were incorporated into receptors in our SH-EP1 cell line. Although varied stoichiometries probably existed in our system (Carbone et al., 2009), specific stoichiometries may exist in vivo. Furthermore, these ratios are functionally relevant. For example, $(\alpha4)_2(\beta2)_3$ nAChRs show higher sensitivity to agonist activation than $(\alpha4)_3(\beta2)_2$ nAChRs (Nelson et al., 2003).

Colocalization of, and efficient intracellular FRET between, α7FP and β2FP implies that an appreciable fraction of the subunits in the ER were coassembled, consistent with prior studies concerning other nAChR subtypes (Grailhe et al., 2004; Drenan et al., 2008). FRET could have been from partially assembled receptors in the ER, but there was no significant difference between E in intracellular regions and

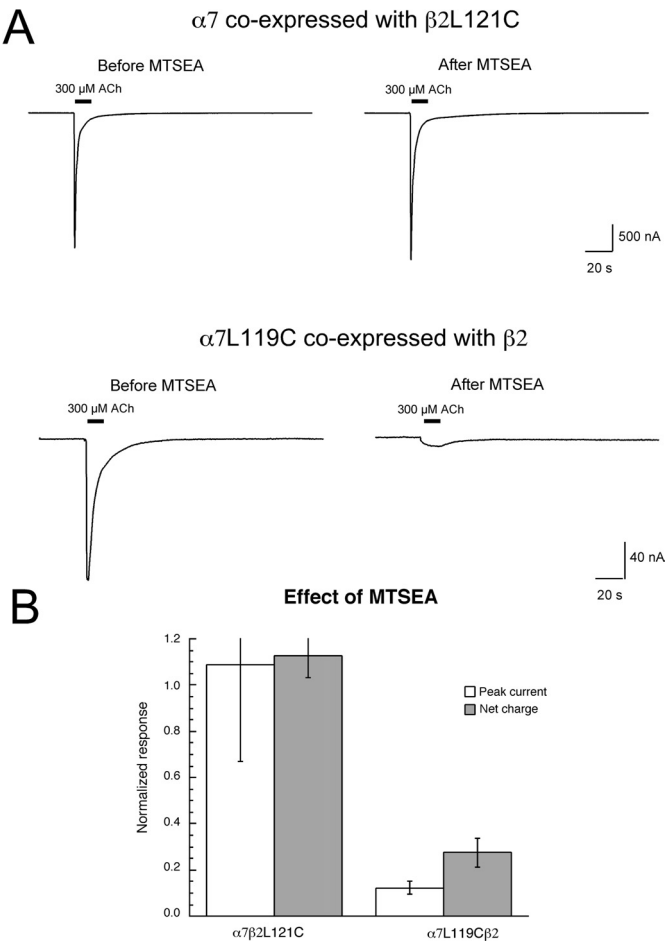

Fig. 7. A, representative traces from oocytes coexpressing either wild-type human $\alpha7$ and human $\beta2^{L121C}$ subunits (upper traces) or human $\alpha7^{L119C}$ and wild-type human $\beta2$ subunits (lower traces). Cells were initially stimulated with 300 μM ACh and then incubated in 2 mM MTSEA for 5 min before the second application of 300 μM ACh. B, the effect of MTSEA treatment on the average peak current and net charge responses of cells expressing $\alpha7\beta2^{L121C}$ nAChRs ($n = 25$) or $\alpha7^{L119C}\beta2$ nAChRs ($n = 6$). Data were normalized to the 300 μM ACh responses obtained from the same cells before MTSEA treatment. All cells were injected with a 4-fold excess of $\beta2$ (wild type or mutant) subunit RNA relative to $\alpha7$ (wild type or mutant) subunit RNA.

in the plasma membrane, which presumably harbors only fully assembled nAChRs (data not shown). These findings are consistent with present concepts that coassembly occurs intracellularly.

TIRF Microscopy Reveals Plasma Membrane Colocalization of FP-Tagged $\alpha7$ and $\beta2$ Subunits. We show for the first time that $\beta2$FP and $\alpha7$FP subunits colocalize in plasma-membrane-rich filopodia-like projections (Fig. 1H), which is consistent with nAChR trafficking to the plasma membrane (Keller et al., 2001). Furthermore, I_n of $\alpha7$Y and $\alpha7Y\beta2C$ nAChR-expressing cells was similar, suggesting that $\beta2$FP subunits did not alter $\alpha7$ subunit localization to filopodia-like processes.

Filopodia, which are common on central nervous system neurons and thought to be precursors of dendritic spines, can receive synapses (Dunaevsky et al., 1999). Moreover, $\alpha7$ nAChRs localize to filopodia of cultured hippocampal neurons (Xu et al., 2006). In addition, FP-labeled $\alpha4\beta2$ nAChRs and 5-HT_{3A} receptors, another Cys-loop receptor, localize to filopodia-like protrusions when expressed in N2a cells (Drenan et al., 2008) and HEK-293 cells (Grailhe et al., 2004), respectively, and localize in dendrites when expressed in primary, midbrain neurons (Nashmi et al., 2003) and cultured hippocampal neurons (Grailhe et al., 2004), respectively. Given the similarities, $\alpha7\beta2$ nAChRs might reasonably be expected to localize to neuronal filopodia and dendrites where expressed, although further studies would be required to test this hypothesis.

Functional Incorporation of the $\beta2$ Subunit into the Receptor Complex. To further examine the putative incorporation of the $\beta2$ subunit into $\alpha7$ receptor complexes, we took advantage of the gain-of-function L9′T mutation as a reporter. Rather than having antagonist activity as it does at wild-type $\alpha7$ nAChRs, DHβE has partial agonist activity at gain-of-function mutant $\alpha7$L9′T receptors. The magnitude of the response to DHβE is reduced upon coexpression with wild-type $\beta3$ subunits, consistent with $\alpha7$L9′T-$\beta3$ subunit coassembly and reduction of the number of the gain-of-function subunits in the pentamer (Palma et al., 1999). Here, we find that DHβE has agonist action only when $\alpha7$ and/or $\beta2$ subunits harbor the L9′T mutation. Inhibition by DHβE was observed upon coexpression of $\alpha7$L9′T and $\beta2$ but not for coexpression of $\alpha7$L9′T and $\beta2$L9′T subunits, which indicates that heteromeric $\alpha7\beta2$ nAChRs are indeed formed.

Likewise, coexpression of the mouse gain-of-function $m\beta2^{V9'S}$ subunit with m$\alpha7$ or m$\alpha7$-YFP subunits significantly altered agonist responses compared with coexpression with wild-type m$\beta2$ subunits confirming $\beta2$ subunit incorporation into functional receptors (Fig. 4; Supplemental Fig. S4; Supplemental Table S2). In addition, by varying the injection ratio of $\alpha7$ to $\beta2$ subunits, we showed a trend toward lower peak current with an increase in $\beta2$ subunit expression. This further suggests that $\beta2$ subunits incorporate into $\alpha7$ nAChRs and that they may not contribute to functional binding sites.

Coexpression of the $\beta2$ Subunit Does Not Modify $\alpha7$ nAChR Pharmacology for Most Agents. Because it is well documented that the functionally relevant ACh binding site lies at the interface between the principal or (+)-face(α) and complementary or (−)-face of specific nAChR subunits, it could be expected that $\beta2$ subunit incorporation into functional $\alpha7$ receptor complexes would yield a receptor with a distinct pharmacological profile having both $\alpha7$-$\beta2$ and $\alpha7$-$\alpha7$ subunit interfaces. Experiments carried out with a series of agonists, the competitive antagonist MLA, and a positive allosteric modulator, however, indicate that $\beta2$ subunit incorporation hardly modifies $\alpha7$ nAChR properties, with the notable exception of lower agonist-induced peak current. In addition, for choline activation, Hill slopes were lower for $\alpha7\beta2$ receptors but only when $\beta2$ was in excess in oocytes ($\alpha7/\beta2$ of 1:10), and for SH-EP1 cells, which, on the basis of our FRET data, also had a higher ratio of $\beta2$ to $\alpha7$ in receptors. This supports the contention that the $\alpha7$-$\beta2$ interface does not bind choline. Also notable was the inhibition of ACh-evoked current for $\alpha7\beta2$ nAChRs by low concentrations of DHβE, which Liu et al. (2009) also observed in putative $\alpha7\beta2$ nAChRs in rodent MS/DB. However, the degree of inhibition was lower for receptors expressed in oocytes, in both the present study and in Liu et al. (2009), which is consistent with a subpopulation of $(\alpha7)_5$ nAChRs. This suggests that cellular mechanisms in MS/DB cells direct $\alpha7$-$\beta2$

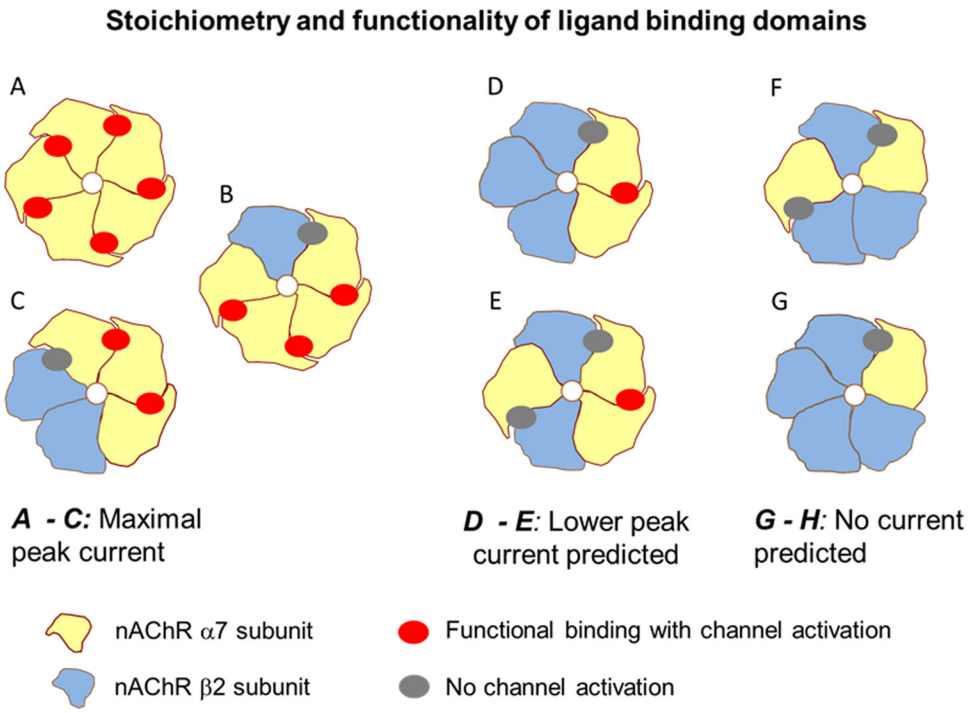

Fig. 8. Stoichiometry and functional binding of agonists: proposed model. Subunits are represented by yellow (α7) and blue (β2) in the model. ACh binding domains that contribute to channel activation are denoted as red ovals and those that do not contribute are denoted as gray ovals. A to C, ACh binds to multiple functional binding domains resulting in maximal peak current. D and E, only one functional ligand binding domain for ACh is likely to result in lower peak current. F and G, no functional ACh binding domains exist; thus, these receptors would be nonfunctional.

coassembly. Future work may elucidate such mechanisms and reveal whether predominant stoichiometries exist.

Cysteine Mutant Reveals That the α7-β2 Interface Does Not Bind Ligand in a Functionally Relevant Manner. Previous work (Papke et al., 2011) identified a leucine (Leu119 in α7, Leu121 in β2) in the complementary face of the agonist binding domain as a potential gatekeeper, able to exclude agonist binding after covalent modification with a cationic sulfhydryl reagent, such as MTSEA. Sulfhydryl modification of a cysteine at this site was equally effective at eliminating the agonist-evoked responses of homomeric $\alpha7^{L119C}$ receptors and heteromeric $\alpha4\beta2^{L121C}$ receptors. In contrast, the agonist-evoked responses of receptors with mutations of the homologous residues in subunits contributing only to the primary face of agonist binding sites (e.g., $\alpha4^{T119C}$), or in obligatory structural subunits such as β3 or α5, were insensitive to sulfhydryl modification. Likewise, although our several lines of evidence indicate that β2 can coassemble with α7 into functional receptors, the insensitivity of $\alpha7\beta2^{L121C}$ receptors to MTSEA indicates that the β2 subunits are not recruited into functional ACh binding sites. This suggests that functional agonist sites in α7β2 heteromers are restricted to the limited number of α7-α7 subunit interfaces. With multiple β2 subunits incorporated into each pentamer, as our data suggest, this would result in a large reduction in the number of potential agonist binding sites, with perhaps no more than a single binding site in each functional receptor. This is consistent with our recent finding (Williams et al., 2011) that under conditions of saturating agonist concentrations, single functional agonist binding sites are sufficient to produce activation of both muscle-type and α7 nAChRs. Indeed, the current evoked by ACh in the present study was modestly reduced when we injected mouse α7 and β2 cRNA in a 1:3 ratio, and it was further reduced for the 1:10 ratio, yet not extinguished. A mixture of stoichiometries and arrangements such as we present in Fig. 8 could account for the graded response we observed.

Prior work (Khiroug et al., 2002; Azam et al., 2003; Liu et al., 2009) suggests that α7β2 nAChRs may be expressed in mammalian brain. The present work confirms that mammalian α7 and β2 subunits form functional receptors and that subunit stoichiometry and arrangement play a role in activating current. On the basis of the lower agonist-evoked current we observed for α7β2 nAChRs, coassembly of β2 into α7* nAChRs in vivo may be a mechanism of functional downregulation. Future heterologous coexpression might provide fruitful models for investigating the effect of drugs and endogenous mechanisms on subunit stoichiometry (Nelson et al., 2003) and further probing α7β2 nAChR sensitivity to amyloid-β (Liu et al., 2009).

Acknowledgments

We thank Dr. Millet Treinin for the gift of the RIC-3 construct, either directly or through Dr. William Green. We thank Dr. Jon Lindstrom for providing the wild-type human nAChR clones for use in constructing the cysteine mutants and Clare Stokes (University of Florida, Gainesville, FL) for creating the cysteine α7 and β2 mutants. We thank Jason Maxwell (Barrow Neurological Institute, Phoenix, AZ) for assistance in producing stably transfected SH-EP1 cell lines and Bhagirathi Dash for creating the gain-of-function mouse β2 construct from a mouse β2 construct kindly provided by Jerry Stitzel. We thank Dr. Christian Fuhrer and Prof. Dr. Ortrud K. Steinlein for providing the human α7 and β2, respectively, and Tanguy Araud and Isabelle Favre (Department of Neuroscience, Centre Médical Universitaire, Geneva, Switzerland) for creating the human α7L9′T and β2L9′T mutants, respectively. In addition, we thank Tanguy Araud, Sonia Bertrand, and Claudette Duret (Department of Neuroscience, Centre Médical Universitaire) and Estelle Neveu (HiQScreen, Geneva, Switzerland) for performing electrophysiological recordings.

Authorship Contributions

Participated in research design: Murray, Bertrand, Papke, George, Pantoja, Srinivasan, Liu, Wu, Whiteaker, Lester, and Lukas.

Conducted experiments: Murray, Bertrand, Papke, George, and Liu.

Performed data analysis: Murray, Bertrand, Papke, George, and Liu.

Wrote or contributed to the writing of the manuscript: Murray, Bertrand, Papke, George, Liu, Whiteaker, Lester and Lukas.

References

Alexander JK, Sagher D, Krivoshein AV, Criado M, Jefford G, and Green WN (2010) Ric-3 promotes α7 nicotinic receptor assembly and trafficking through the ER subcompartment of dendrites. *J Neurosci* **30:**10112–10126.

Anand R, Peng X, and Lindstrom J (1993) Homomeric and native α7 acetylcholine receptors exhibit remarkably similar but non-identical pharmacological properties, suggesting that the native receptor is a heteromeric protein complex. *FEBS Lett* **327:**241–246.

Azam L, Winzer-Serhan U, and Leslie FM (2003) Co-expression of α7 and β2 nicotinic acetylcholine receptor subunit mRNAS within rat brain cholinergic neurons. *Neuroscience* **119:**965–977.

Bertrand D, Devillers-Thiéry A, Revah F, Galzi JL, Hussy N, Mulle C, Bertrand S, Ballivet M, and Changeux JP (1992) Unconventional pharmacology of a neuronal nicotinic receptor mutated in the channel domain. *Proc Natl Acad Sci USA* **89:** 1261–1265.

Bohler S, Gay S, Bertrand S, Corringer PJ, Edelstein SJ, Changeux JP, and Bertrand D (2001) Desensitization of neuronal nicotinic acetylcholine receptors conferred by N-terminal segments of the β2 subunit. *Biochemistry* **40:**2066–2074.

Carbone AL, Moroni M, Groot-Kormelink PJ, and Bermudez I (2009) Pentameric concatenated $(\alpha4)_2(\beta2)_3$ and $(\alpha4)_3(\beta2)_2$ nicotinic acetylcholine receptors: subunit arrangement determines functional expression. *Br J Pharmacol* **156:**970–981.

Chavez-Noriega LE, Crona JH, Washburn MS, Urrutia A, Elliott KJ, and Johnson EC (1997) Pharmacological characterization of recombinant human neuronal nicotinic acetylcholine receptors hα2β2, hα2β4, hα3β2, hα3β4, hα4β2, hα4β4 and hα7 expressed in *Xenopus* oocytes. *J Pharmacol Exp Ther* **280:**346–356.

Couturier S, Bertrand D, Matter JM, Hernandez MC, Bertrand S, Millar N, Valera S, Barkas T, and Ballivet M (1990) A neuronal nicotinic acetylcholine receptor subunit (α7) is developmentally regulated and forms a homo-oligomeric channel blocked by α-BTX. *Neuron* **5:**847–856.

Deneris ES, Connolly J, Boulter J, Wada E, Wada K, Swanson LW, Patrick J, and Heinemann S (1988) Primary structure and expression of β2: a novel subunit of neuronal nicotinic acetylcholine receptors. *Neuron* **1:**45–54.

Drenan RM, Nashmi R, Imoukhuede P, Just H, McKinney S, and Lester HA (2008) Subcellular trafficking, pentameric assembly, and subunit stoichiometry of neuronal nicotinic acetylcholine receptors containing fluorescently labeled α6 and β3 subunits. *Mol Pharmacol* **73:**27–41.

Dunaevsky A, Tashiro A, Majewska A, Mason C, and Yuste R (1999) Developmental regulation of spine motility in the mammalian central nervous system. *Proc Natl Acad Sci USA* **96:**13438–13443.

Francis MM and Papke RL (1996) Muscle-type nicotinic acetylcholine receptor delta subunit determines sensitivity to noncompetitive inhibitors, while gamma subunit regulates divalent permeability. *Neuropharmacology* **35:**1547–1556.

Gotti C, Hanke W, Maury K, Moretti M, Ballivet M, Clementi F, and Bertrand D (1994) Pharmacology and biophysical properties of α7 and α7-α8 α-bungarotoxin receptor subtypes immunopurified from the chick optic lobe. *Eur J Neurosci* **6:**1281–1291.

Grailhe R, de Carvalho LP, Paas Y, Le Poupon C, Soudant M, Bregestovski P, Changeux JP, and Corringer PJ (2004) Distinct subcellular targeting of fluorescent nicotinic $\alpha4\beta3$ and serotoninergic 5-HT3A receptors in hippocampal neurons. *Eur J Neurosci* **19:**855–862.

Halevi S, Yassin L, Eshel M, Sala F, Sala S, Criado M, and Treinin M (2003) Conservation within the RIC-3 gene family. Effectors of mammalian nicotinic acetylcholine receptor expression. *J Biol Chem* **278:**34411–34417.

Hogg RC, Bandelier F, Benoit A, Dosch R, and Bertrand D (2008) An automated system for intracellular and intranuclear injection. *J Neurosci Methods* **169:**65–75.

Keller SH, Lindstrom J, Ellisman M, and Taylor P (2001) Adjacent basic amino acid residues recognized by the COP I complex and ubiquitination govern endoplasmic reticulum to cell surface trafficking of the nicotinic acetylcholine receptor α-subunit. *J Biol Chem* **276:**18384–18391.

Khakh BS, Fisher JA, Nashmi R, Bowser DN, and Lester HA (2005) An angstrom scale interaction between plasma membrane ATP-gated $P2X_2$ and $\alpha_4\beta_2$ nicotinic channels measured with fluorescence resonance energy transfer and total internal reflection fluorescence microscopy. *J Neurosci* **25:**6911–6920.

Khiroug SS, Harkness PC, Lamb PW, Sudweeks SN, Khiroug L, Millar NS, and Yakel JL (2002) Rat nicotinic ACh receptor α7 and β2 subunits co-assemble to form functional heteromeric nicotinic receptor channels. *J Physiol* **540:**425–434.

Lansdell SJ, Gee VJ, Harkness PC, Doward AI, Baker ER, Gibb AJ, and Millar NS (2005) RIC-3 enhances functional expression of multiple nicotinic acetylcholine receptor subtypes in mammalian cells. *Mol Pharmacol* **68:**1431–1438.

Le Novère N, Corringer PJ, and Changeux JP (2002) The diversity of subunit composition in nachrs: evolutionary origins, physiologic and pharmacologic consequences. *J Neurobiol* **53:**447–456.

Lester HA, Dibas MI, Dahan DS, Leite JF, and Dougherty DA (2004) Cys-loop receptors: new twists and turns. *Trends Neurosci* **27:**329–336.

Liu Q, Huang Y, Xue F, Simard A, DeChon J, Li G, Zhang J, Lucero L, Wang M, Sierks M, et al. (2009) A novel nicotinic acetylcholine receptor subtype in basal forebrain cholinergic neurons with high sensitivity to amyloid peptides. *J Neurosci* **29:**918–929.

Luetje CW and Patrick J (1991) Both α- and β-subunits contribute to the agonist sensitivity of neuronal nicotinic acetylcholine receptors. *J Neurosci* **11:**837–845.

Lukas RJ and Bencherif M (2006) Recent developments in nicotinic acetylcholine receptor biology, in *Biological and Biophysical Aspects of Ligand-Gated Ion Channel Receptor Superfamilies* (Arias H ed) pp 27–59, Research Signpost, Kerala, India.

Marks MJ, Whiteaker P, Calcaterra J, Stitzel JA, Bullock AE, Grady SR, Picciotto MR, Changeux JP, and Collins AC (1999) Two pharmacologically distinct components of nicotinic receptor-mediated rubidium efflux in mouse brain require the β2 subunit. *J Pharmacol Exp Ther* **289:**1090–1103.

Murray TA, Liu Q, Whiteaker P, Wu J, and Lukas RJ (2009) Nicotinic acetylcholine receptor α7 subunits with a C2 cytoplasmic loop yellow fluorescent protein insertion form functional receptors. *Acta Pharmacol Sin* **30:**828–841.

Nashmi R, Dickinson ME, McKinney S, Jareb M, Labarca C, Fraser SE, and Lester HA (2003) Assembly of $\alpha4\beta2$ nicotinic acetylcholine receptors assessed with functional fluorescently labeled subunits: effects of localization, trafficking, and nicotine-induced upregulation in clonal mammalian cells and in cultured midbrain neurons. *J Neurosci* **23:**11554–11567.

Nelson ME, Kuryatov A, Choi CH, Zhou Y, and Lindstrom J (2003) Alternate stoichiometries of $\alpha4\beta2$ nicotinic acetylcholine receptors. *Mol Pharmacol* **63:**332–341.

Palma E, Maggi L, Barabino B, Eusebi F, and Ballivet M (1999) Nicotinic acetylcholine receptors assembled from the α7 and β3 subunits. *J Biol Chem* **274:**18335–18340.

Papke RL and Porter-Papke JK (2002) Comparative pharmacology of rat and human α7 nAChR conducted with net charge analysis. *Br J Pharmacol* **137:**49–61.

Papke RL, Stokes C, Williams DK, Wang J, and Horenstein NA (2011) Cysteine accessibility analysis of the human α7 nicotinic acetylcholine receptor ligand-binding domain identifies L119 as a gatekeeper. *Neuropharmacology* **60:**159–171.

Revah F, Bertrand D, Galzi JL, Devillers-Thiéry A, Mulle C, Hussy N, Bertrand S, Ballivet M, and Changeux JP (1991) Mutations in the channel domain alter desensitization of a neuronal nicotinic receptor. *Nature* **353:**846–849.

Slimko EM and Lester HA (2003) Codon optimization of *Caenorhabditis elegans* GluCl ion channel genes for mammalian cells dramatically improves expression levels. *J Neurosci Methods* **124:**75–81.

Stokes C, Papke JK, Horenstein NA, Kem WR, McCormack TJ, and Papke RL (2004) The structural basis for GTS-21 selectivity between human and rat nicotinic α7 receptors. *Mol Pharmacol* **66:**14–24.

Williams DK, Stokes C, Horenstein NA, and Papke RL (2011) The effective opening of nicotinic acetylcholine receptors with single agonist binding sites. *J Gen Physiol* **137:**369–384.

Wu J, Liu Q, Yu K, Hu J, Kuo YP, Segerberg M, St John PA, and Lukas RJ (2006) Roles of nicotinic acetylcholine receptor β subunits in function of human α4-containing nicotinic receptors. *J Physiol* **576:**103–118.

Xu J, Zhu Y, and Heinemann SF (2006) Identification of sequence motifs that target neuronal nicotinic receptors to dendrites and axons. *J Neurosci* **26:**9780–9793.

Zarei MM, Radcliffe KA, Chen D, Patrick JW, and Dani JA (1999) Distributions of nicotinic acetylcholine receptor α7 and β2 subunits on cultured hippocampal neurons. *Neuroscience* **88:**755–764.

Address correspondence to: Dr. Teresa A. Murray, Louisiana Tech University, Biomedical Engineering Center, PO Box 10157, Ruston, LA 71272-0046. E-mail: bioengineer1@hotmail.com